Sensors and Materials, Vol. 13, No. 1 (2001) 025–040
MYU Tokyo

S & M 0427

Miniaturized Magnetic Field Sensors Utilizing Giant Magneto-Impedance [GMI] Effect and Surface Acoustic Wave [SAW] Technology

H. Hauser*,**, R. Steindl, Ch. Hausleitner, J. Nicolics and A. Pohl

Institute of Industrial Electronics and Material Science,
Vienna University of Technology, Guβhausstraβe 27–29/366, A–1040 Vienna, Austria

(Received March 6, 2000; accepted January 9, 2001)

Keywords: magnetic field sensor, giant magneto-impedance (GMI) effect, surface acoustic wave (SAW) device, amorphous FeCoSiBNd wire, tire wear sensor

Based on the giant magneto-impedance (GMI) effect in 30-μm-diameter amorphous FeCoSiBNd wires with very low magnetostriction, two types of micromagnetic field sensors are developed. Consisting of 30–100-μm-long samples, a GMI read-head was integrated into a frequency modulation circuit by laser microwelding. Reproducible measurements of the surface flux distribution of a mechanically structured magnetic barcode were carried out in order to demonstrate the performance. Furthermore, a new type of surface acoustic wave (SAW) device employs the electrical load of the SAW device by the impedance of conventional sensors. In order to develop a wirelessly interrogable magnetic field sensor, the combination of GMI sensors and SAW transponders is discussed and a prototype is characterized by several measurements, including an application as a tire wear sensor. Both sensor types show a high sensitivity with a resolution of 100 nT for dc fields and a bandwidth of more than 10 MHz.

1. Introduction

The principles and basic characteristics of the GMI effect and SAW technology are demonstrated by the investigation of two types of micromagnetic sensors. Microscale magnetic sensors with high sensitivity, quick response, and high temperature stability are needed for recent developments such as magnetic recording technology, highly accurate rotary encoding for intelligent robot control, and nondestructive testing and sensing in various industrial, automotive, and environmental measurement tasks.

*Corresponding author, e-mail address: Hans.Hauser@TUwien.ac.at
**Invited paper

For such applications, anisotropic magnetoresistance (AMR) elements have been widely used as micromagnetic heads and micromagnetic sensors.[1] However, the AMR element is predicted to become obsolete for further high-density magnetic disks due to its low signal-to-noise ratio (with an AMR ratio of 2–4%[2] for a field of 2–4 mT, about 1%/mT).

Giant magnetoresistance (GMR)[3] is a promising phenomenon for the development of a new micromagnetic head due to its higher GMR ratio of 4% for about 400 μT (about 10%/mT) as a spin valve sensor. However, more sensitive microelements will be required in the near future for high-resolution magnetic measurements, *e.g.*, for reading magnetic barcodes.[4]

The impedance of a high-permeability element sensitively changes with an external (quasistatical) field due to the skin effect in a high-frequency current application. This GMI effect[5,6] shows an extremely high impedance ratio of 100–1200%/mT in zero-magnetostrictive amorphous wires. In addition, the magnetovoltage of a GMI element in a self-oscillation circuit such as a Colpitts oscillator shows a high changing ratio of the element voltage amplitude, five- to sixfold larger than the GMI ratio. Another important feature of the GMI element is its independence of the demagnetizing field with respect to the external field. This feature allows the construction of a microscale head without decreasing the field-detection sensitivity due to the circumferential magnetization with the element current. Quick response is also an advantageous point of the GMI effect due to the high-frequency current magnetization which works as a carrier of the amplitude or frequency modulation behavior.

2. Giant Magneto-Impedance Effect

The following section describes the physical origin of the GMI effect in thin wires and thin films. The theoretical considerations are mainly based on the works of Mohri and Panina; for example, see ref. 7.

Depending on the frequency $f = \omega / 2\pi$, the impedance Z is the ratio of complex ac voltage U and complex ac current I. It is expressed in a ferromagnetic wire (with resistivity ρ, radius r and length l and for $\delta \ll r$) as

$$Z = R_{dc}\frac{r}{2\delta} + j\omega L_i \frac{2\delta}{r} = (1+\mathrm{j})\frac{l}{2\pi r}\sqrt{\frac{\omega\mu\rho}{2}}, \tag{1}$$

and the voltage is $|U| = |Z| \cdot |I| = |I| \cdot \sqrt{\omega\mu\rho}\, l / 2\pi r$, where $\delta = \sqrt{2\rho / \omega\mu}$ is the skin depth, $R_{dc} = \rho l/\pi r^2$ is the dc resistance, $L_i = \mu l/8\pi$ is the internal inductance, $\mu = \mu_{dc}/(1 + \mathrm{j}f_r/f)$ is the complex circumferential permeability, μ_{dc} is the relative dc permeability, and f_r is the domain wall relaxation frequency, which finally depends on the applied external field H_a. The effective susceptibility $\kappa_{eff} = \mu/\mu_0 + 1$ consists of contributions of domain wall displacements (susceptibility κ_D), which dominate at low frequencies, and contributions of magnetization rotation (susceptibility κ_R), which dominate at high frequencies: $\kappa_{eff} = \kappa_R + \kappa_D$. As the magnetic structure strongly depends on the magnetic anisotropy of the material, this

feature determines the GMI characteristics. The skin effect appears in the wire at a current of more than 200 kHz. The voltage amplitude U_a is proportional to ω and μ, as expressed above. Therefore, the average differential permeability in the circumferential direction due to 180° domain wall oscillation decreases with increasing external applied dc field H_a at a relatively low-frequency (1 MHz) magnetization without dc bias current, in which the magnetization vector in each domain gradually declines with increasing H_a and the relative change

$$\xi = \frac{U_a(H_a) - U_a(0)}{U_a(0)}, \tag{2}$$

is about –130%/mT. Applying a dc bias field (bias current) increases U_a with increasing H_a in low fields due to the increase of μ. U_a vs H_a characteristics are always of V-character shape at f = 10 MHz at which the domain wall movement is strongly suppressed due to a large eddy-current damping; the magnitude of μ increases with increasing H_a in the low H_a region until H_a is about $\mu_0 H_k$ (anisotropy field) with a magnetization rotation. A very high sensitivity value up to 1200%/mT is obtained with a full dc bias which can also be applied by a small permanent magnet.

3. Shape Anisotropy

Shape effects are an important consideration in the design of magnetic sensors. The direction sensitivity is mainly determined by the shape anisotropy energy. A spontaneously magnetized body exhibits fictitious magnetic charges (north (+) and south (–) poles) at the surface, where the normal component of $\vec{M}$ is discontinous. These magnetic poles are considered as the origin of a magnetic field $\vec{H}_d$, proportional to the magnetization $\vec{M}$ (see Fig. 1) and are oriented antiparallel to the magnetization within the magnetized body. (As real magnetic charges do not exist, the field H_d originates from the moving electrical charges producing the magnetic moments of density M.) The energy density of the so-called demagnetizing field of a general ellipsoid is

$$\omega_D = \frac{\mu_0 M^2}{2}\left(N_a\alpha_1^{\,2} + N_b\alpha_2^{\,2} + N_c\alpha_3^{\,2}\right), \tag{3}$$

where N_a, N_b, and N_c are the demagnetizing factors ($N_a + N_b + N_c = 1$) and α_i are the direction cosines of the magnetization with respect to the ellipsoid axes a, b and c. The energy areas[8] of eq. (3) show that ω_D is minimum at the axis of a bar or in the plane of a disc (see Fig. 2). The magnetic fields are only homogeneous in an ellipsoid. In this case, the demagnetizing matrix $\underline{N}_d = (N_a, N_b, N_c)$ defined by $\vec{H}_d = -\underline{N}_d \cdot \vec{M}$ can be calculated

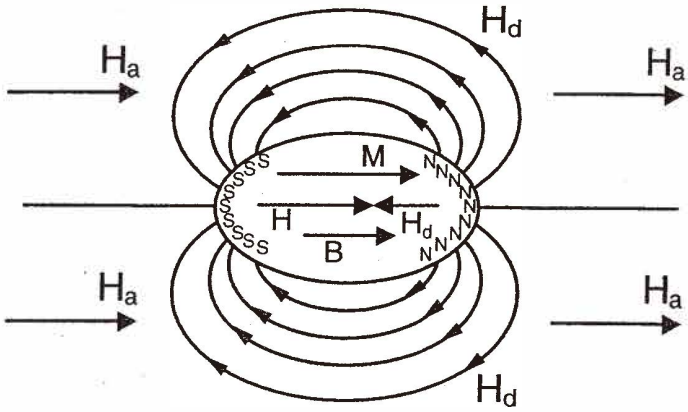

Fig. 1. Demagnetizing field of a magnetized ellipsoid.

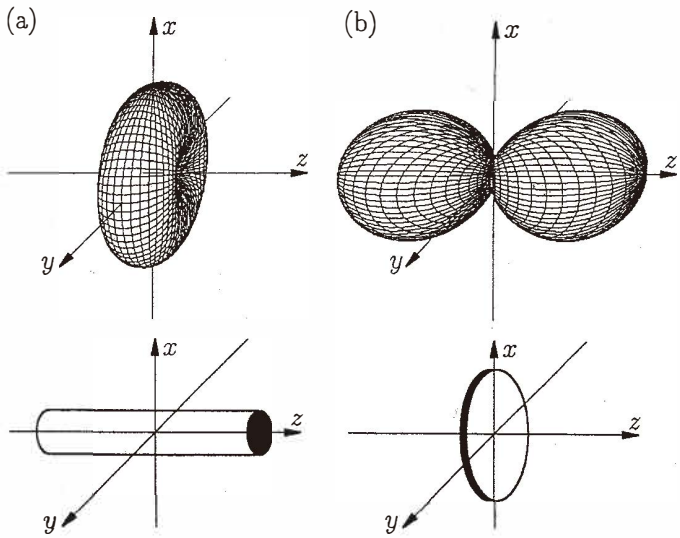

Fig. 2. Demagnetizing stray field energy of ellipsoid approximations; long bar (a) and flat disc (b).

analytically. Otherwise, it has a very complex structure and depends on the actual susceptibility. If the field H_a is applied, the inner, effective field $\vec{H} = \vec{H}_a + \vec{H}_d$ differs from H_a by H_d. In simplified cases of only one anisotropy constant K it is also usual to define a fictitious anisotropy field, $H_k = 2\,K/\mu_0 M_s$. In the case of a long, thin wire ($N_a = N_b \gg N_c$), the

anisotropy field is $H_k \approx M_s (N_a - N_c)$. For the given material and geometry (spontaneous magnetization $M_s = 560$ kA/m, $N_a = 0.47$, $N_b = 0.06$) the maximum anisotropy field is $H_k = 230$ kA/m, which is only valid for the single domain case.

4. Micromagnetic Read-Head for Magneto-Mechanical Barcode

Sensitive and quick-response micromagnetic sensors have been investigated using a GMI wire installed in a Colpitts oscillation circuit by laser welding, followed by a detector (demodulation) and a differential amplifier. These microsensors with 30–100-μm-long amorphous wire heads exhibit a sensitivity of about 1 V/mT, depending on a magnetic bias field, and a bandwidth of 10 MHz.[9]

Figure 3 illustrates the sensor head schematically and includes a photograph of a realized structure. The thermal capacity of the copper stripes ensures a good cooling performance during the Nd:Yttrium Aluminum Garnet (YAG) pulsed laser welding process.

Figure 4 shows the scheme of the electronic circuit of a GMI sensor. Both the amplitude and frequency of the resonant circuit voltage sensitively increase with increasing external field $B_a = \mu_0 H_a$ (frequency modulation). The signal as a measure of the field is obtained by demodulation using standard Frequency Modulation (FM) receiver technology. The dc bias was supplied by a small permanent magnet.

The voltage-amplitude U_a vs the dc external field B_a characteristics in a FeCoSiBNd zero-magnetostrictive (magnetostriction constant $\lambda = -10^{-7}$) amorphous wire with 30 μm diameter and 70 μm length magnetized with a high-frequency current of 100 MHz are shown in Fig. 5.

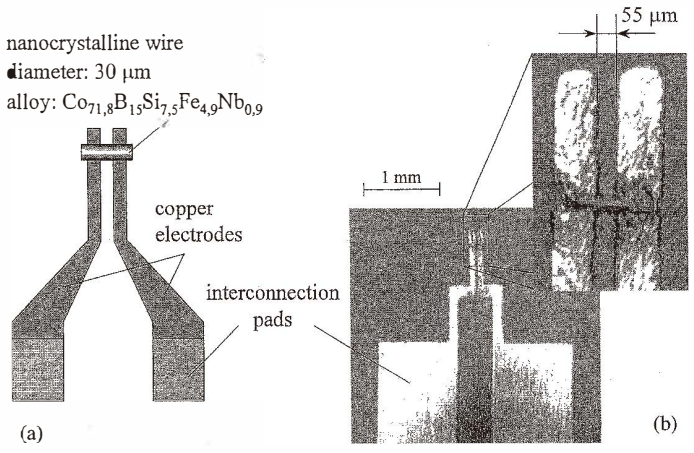

Fig. 3. Micromagnetic sensor head; (a) schematic illustration, (b) photograph of a prototype head.

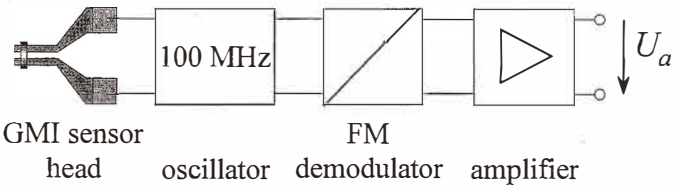

Fig. 4. Schematic electronic arrangement; Sensor with bias permanent magnet, 100 MHz oscillator, FM-radio demodulator, and dc amplifier (output voltage U_a).

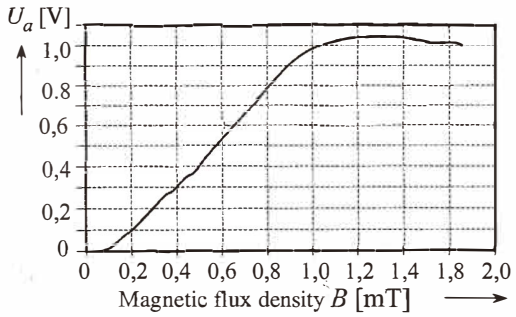

Fig. 5. Output voltage U_a vs flux density B_a of the GMI sensor.

Figure 6 depicts a widely used mechanically coded magnetic structure for a control system.[10] The result of a reading experiment on a barcode layer shown in Fig. 6 is illustrated in Fig. 7. The short spacing of the sensitive wire length ensures a large angle area of more than ±70° (of the wire axis with respect to the barcode stripe) for reliable signal detection.[11]

5. Passive SAW Sensors and Transducers

SAW devices have been well known for more than three decades.[12] They utilize the propagation of an acoustic wave on the surface of a plain polished piezoelectric substrate. SAW devices have been introduced for filters and as frequency reference elements, as well as for signal processing in communications engineering. During device design, in order to achieve stable reference elements, the electrical parameters have been kept as insensitive as possible to the environmental conditions.

On the other hand, for sensor applications, the effect of a measurand on the propagation of the SAW due to an effect on the elastic constants of the substrate is utilized. Sensors for many tasks in laboratories and industries have been presented in the last decade. Employ-

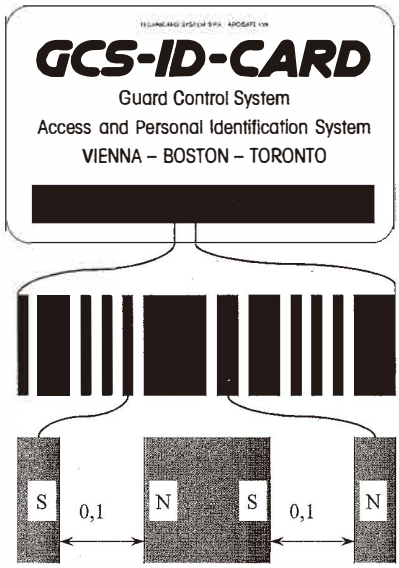

Fig. 6. Schematic structure of a magnetic barcode example.

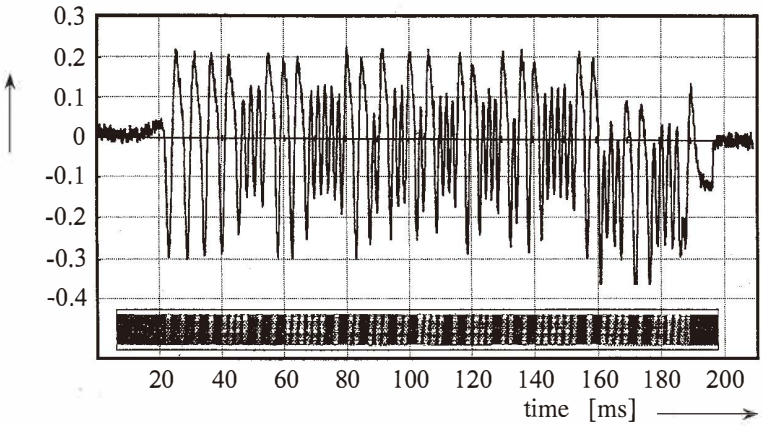

Fig. 7. Output voltage U_a vs time during the reading process of a magnetic barcode stripe.

ing a one-port SAW device and connecting the electrical port to an antenna yields passive, wirelessly interrogable sensor elements. The measurand affects the delay and the resonance frequency, respectively. The sensor responds to a radio-frequency (RF) signal, and information about the measurand can be gained from the RF response signal ("request" is used hereafter for this procedure).[13]

Passive SAW radio sensors are known to be completely maintenance-free and resistant to severe environmental conditions such as high temperature, high electric and magnetic field strength, and even hard radiation. Since the measurand is evaluated from the RF response signal, which is disturbed by noise and interference, the required signal processing increases the complexity of such systems. For applications where a wired connection to the sensor and/or an active radio sensor containing semiconductor devices cannot be used for the reasons stated above, SAW sensors represent an appropriate choice. With the measurand affecting the SAW substrate directly, they are capable of the remote measurement of temperature as well as torque, identification, and pressure.

A new passive SAW sensor has recently been presented,[14] in which a two-port SAW device is used as a transponder which is loaded by external impedance. A change in impedance varies the reflectivity of the reflector in magnitude and phase to be read out by the radio request system. The information on external impedance modulates an individual part of the sensor response. A conventional stock sensor can be used as the passive sensor unit in such SAW transponders. In Fig. 8, the scheme of these circuits is drawn.

The SAW arriving at an interdigital transducer (IDT) generates a charge distribution and therefore an electric voltage between the fingers, reexciting the SAW. If the charge is short-circuited, no reflection will occur. This acoustic reflectivity of an IDT as a function of a complex termination impedance Z_{load} at its electrical ports is given in the well-known P-matrix formalism with P_{11} :

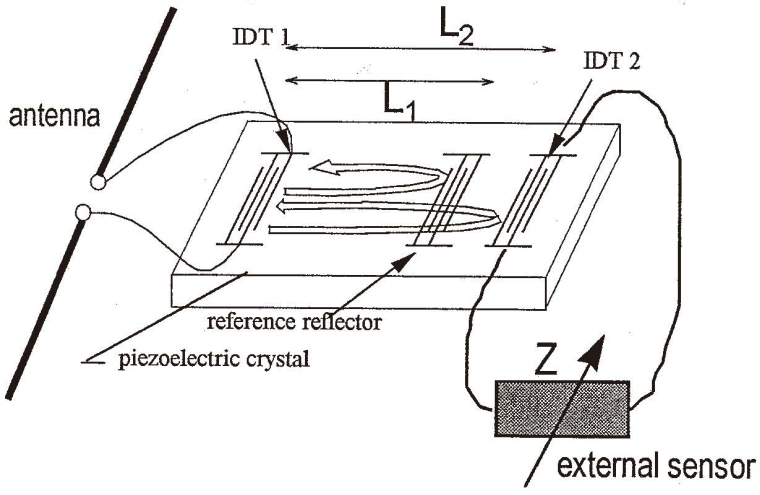

Fig. 8. Schematic layout of a two-port SAW transponder with an external stock sensor.

$$P_{11}(Z_{load}) = P_{11}^{sc} + \frac{2P_{13}^2}{P_{33} + \frac{1}{Z_{load}}}, \tag{4}$$

The optimum short-circuit (index sc) is achieved by a serial resonance, where the electrical load Z_{load} consists of a serial circuit of an impedance (resistive, capacitive or inductive) with the inductance of the bonding and connecting wires. The smaller the bonding inductance, the further the short-circuit point moves towards the origin. The open-point is determined by the IDT of the SAW device (by the matrix elements P_{13} and P_{33}).

As shown in eq. (4), the external load impedance modulates the reflected RF impulse in magnitude and phase. As calculated in eq. (13), the information can be gained with high resolution by phase measurement. If a maximum resolution of ≈1% is sufficient, only a discrimination of the amplitude can be performed. In Fig. 9, the amplitude is depicted for a capacitive sensor with a fixed serial inductance. For the 30-nH inductor, a serial resonance at the operation frequency of 433 MHz is achieved for a capacitance of 4.5 pF. Here, a maximum dynamic range but ambiguous readout is achieved.

The dynamic range for an actual setup is up to 30 dB, representing an amplitude ratio of ≈30. Depending on the received noise level, the resolution stated above can be achieved. An estimation of the resulting error for different types of error sources is comprehensively

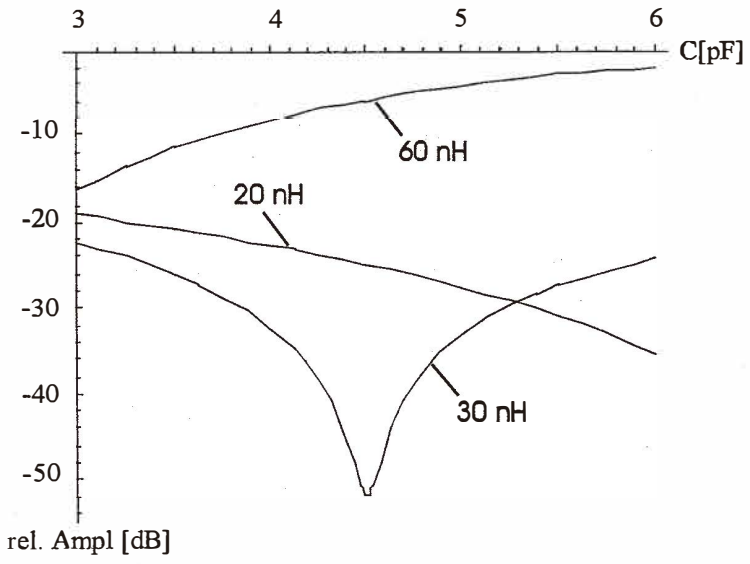

Fig. 9. Relative amplitude of the reflected impulse vs capacitance of a sensor with the parameter of fixed inductance.

summarized in ref. 15. The measurement process implemented employs differential measurement of amplitude and phase of the response signal. The signal reflected by the reference reflector is compared with that from the IDT connected to the external sensor.

6. GMI and SAW

A new wirelessly interrogable sensor for magnetic fields can be achieved, establishing an alliance between the new GMI sensors and SAW transponder devices. Therefore, the GMI device is coupled to the second port (IDT2 in Fig. 8) of the SAW transponder. The circuit is adjusted to achieve resonance with the transducer's capacitance. Tuning the resonance to one octave in frequency by applying a magnetic field to the GMI sensor yields a sufficient effect for a radio request readout. Passive, radio-requestable current sensors can be built. First results have been reported recently;[9] now we present more details of the sensor circuits and applications.

6.1 *Magnetic field sensor*

In Fig. 10, the variation of resistance and inductance of the GMI wire vs the magnetic field strength is depicted. For a frequency of 433 MHz, the variation of the inductance is between 20 and ≈100 nH for an applied field B_a between 0.0 T and 0.4 T. The comparison of the results in Fig. 10 and the calculation[9,11] yields that the combination of a 13-mm-long GMI element with a serial capacitor of 6 pF represents an external impedance load which can be matched to a typical 433 MHz SAW reflector IDT and thus a wirelessly interrogable passive sensor for magnetic field measurement is realized.

A prototype based on the principle sketched in Fig. 11 was built and tested. The results, the amplitude A_{IDT2} of the affected reflector relative to the reference reflector amplitude A_{ref} (see Fig. 8), are shown in Fig. 12. This relative amplitude is defined as

$$A_{rel}[\mathrm{dB}] = 20 \log \left| \frac{A_{IDT2}}{A_{ref}} \right| . \tag{5}$$

The measurements reflect the theoretical behavior based on eq. (4). From Fig. 12, it is evident that the principle is best suited for applications where a magnetic field must be measured without contact and where a power supply to the sensor is not feasible. The sensitivity (relative signal amplitude/B_a) is 80 dB/T in the region of weak fields (up to 30 mT). The measurements have been carried out using a GMI wire arrangement produced similarly to the specimen shown in Fig. 3.

6.2 *Tire wear sensor*

First results are obtained from an application as a tire wear sensor. To measure the wear of a vehicle tire a magnetic field sensor as described before is used.[16] The dc external field $B_0 = \mu_0 H_0$ for the GMI wire is generated by one tread element of the wear layer. Therefore,

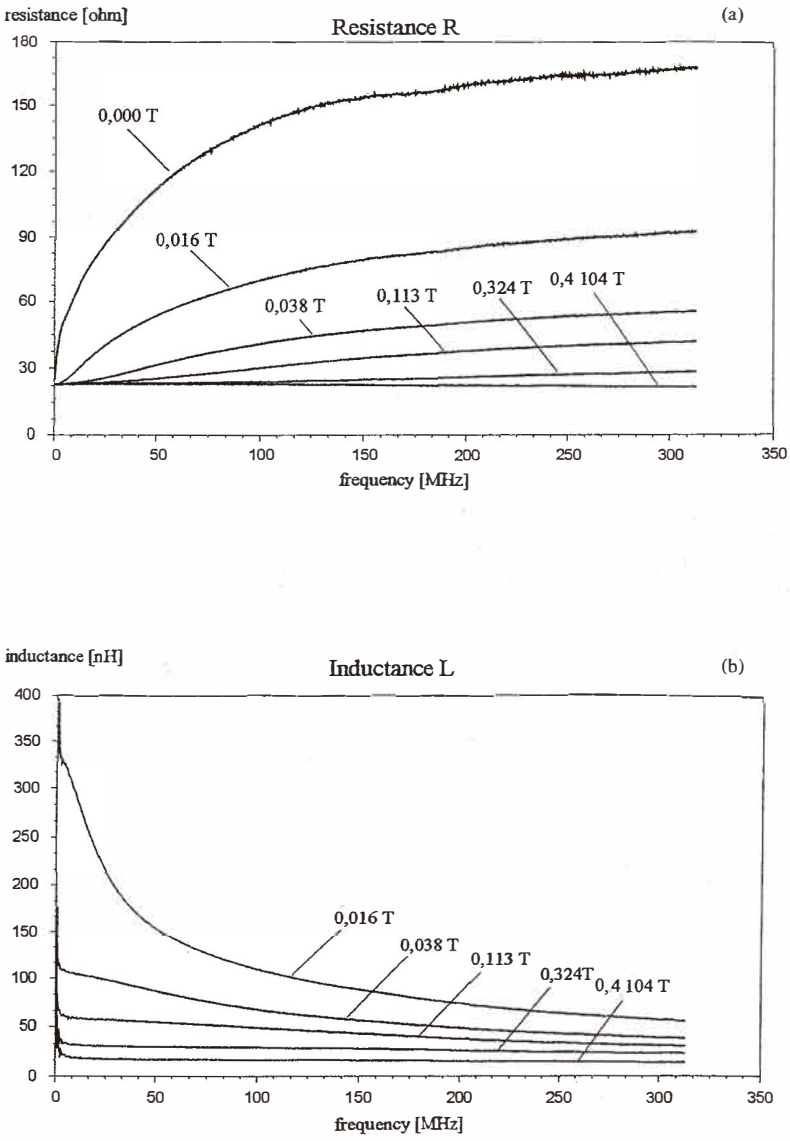

Fig. 10. Resistance (a) and inductance (b) of a 13-mm-long GMI wire vs applied magnetic field.

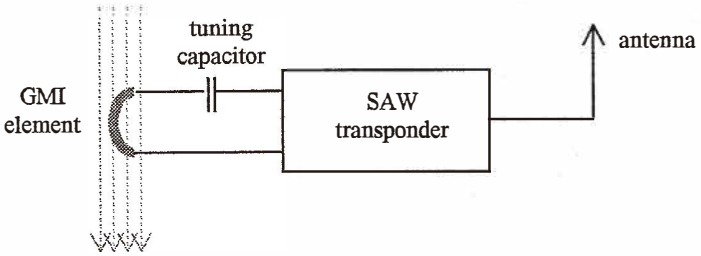

Fig. 11. Wirelessly interrogable passive magnetic field sensor.

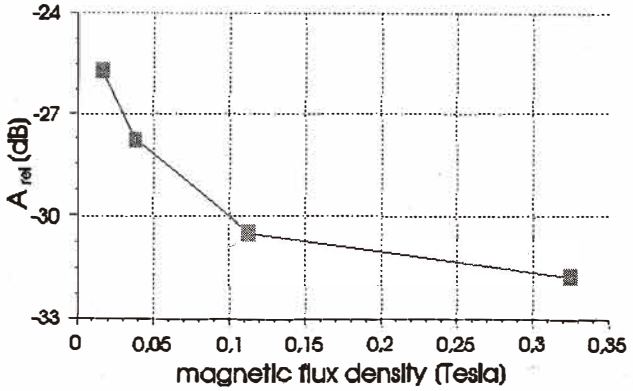

Fig. 12. Amplitude of the impedance-affected reflection relative to the reference.

magnetizeable particles are mixed in the rubber of this element. If the tread decreases, the magnetic field B_0 also decreases. A schematic diagram of the tire wear sensor is shown in Fig. 13.

To optimize the matching network for the SAW transponder, we measured the impedance Z of the GMI wire at 433 MHz as a function of tread depth to determine a mathematical approximation for the reflection coefficient r (h in mm):

$$r(h) = 0.53\exp(j \log_{20}[0.7h + 0.7], \tag{6}$$

with

$$r = \frac{Z - Z_0}{Z + Z_0}, \tag{7}$$

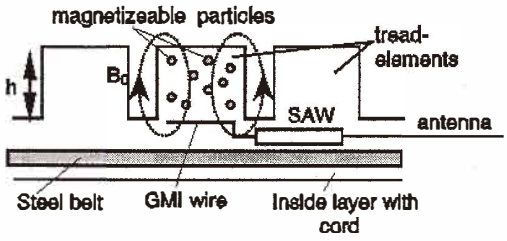

Fig. 13. Schematic diagram of the tire wear sensor.

and $Z_0 = 50\ \omega$. In Fig. 14, the calculated impedance of the GMI wire with a tread depth from 0.0 to 6.6 mm is drawn into an impedance Smith chart. In addition, some measured points are shown.

Due to the low impedance range of the GMI wire it is necessary to find a matching network for the maximum dynamic range of the reflectivity of the IDT2 with eq. (7). Figure 15 shows the best-suited solution with $C = 5$ pF, $L = 17$ nH, and the length of the impedance transformation waveguide line of 1.3 rad. The achieved dynamic range is 7.4 dB and the calculated result is shown in Fig. 16.

Because this line is quite long, and in most applications it is necessary to build small sensors, we used a L/C matching network, which is shown in Fig. 17. With $C = 6.6$ pF and $L = 10$ nH, we calculated a dynamic range of 6 dB. We achieved a smallest inductance of 16 nH in the setup. The relative amplitude of the reflected impulse vs the tread depth is shown in Fig. 18. The theoretical results with 16 nH are compared to experimental measurements, showing good correspondence. The "ideal" solution with 10 nH is also drawn in Fig. 18.

7. Conclusion and Outlook

The giant magneto-impedance effect element shows a high sensitivity based on large impedance changes with an external magnetic field, using resonant circuit technology. A quick-response microscale magnetic sensor is investigated for highly reliable measurements of the stray fields of magnetic barcodes. The high shape anisotropy also enables a high directional sensitivity. Furthermore, the laser welding process is suitable for industrial low-cost mass fabrication.

SAW transponders have been developed to operate as reliable passive wirelessly interrogable sensors in hostile environments with no need of a power supply but an almost unlimited lifetime. New SAW transponders combine the advantages of SAW technology and conventional stock sensor elements with a measurand-dependent impedance. The performance of the passive wirelessly interrogable SAW sensor prototype is very promising. The application as a tire wear sensor represents the typical advantages of passive, wireless sensors. The evaluation of a passive radio sensor for electric current, *e.g.*, at high tension lines, is in progress. The next step in the development is the introduction of GMI films in SAW substrates to achieve integrated sensor devices.

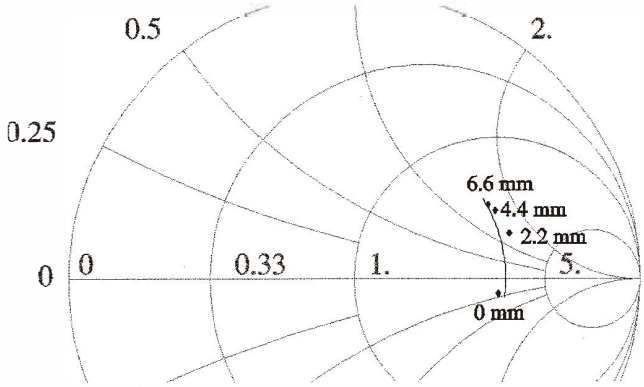

Fig. 14. Impedance of the GMI wire (measured points and approached function).

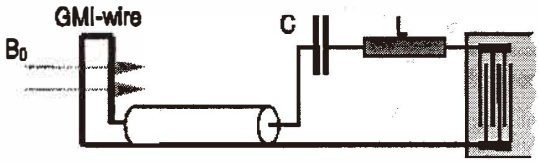

Fig. 15. Matching network for maximum dynamic range.

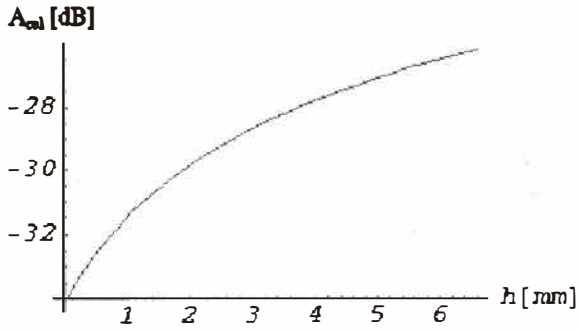

Fig. 16. Amplitude of the impedance-affected impulse relative to the reference impulse.

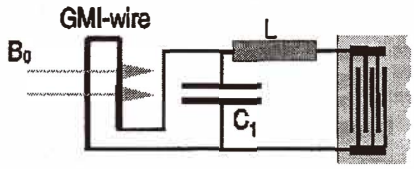

Fig. 17. Simplified matching network for good dynamic range.

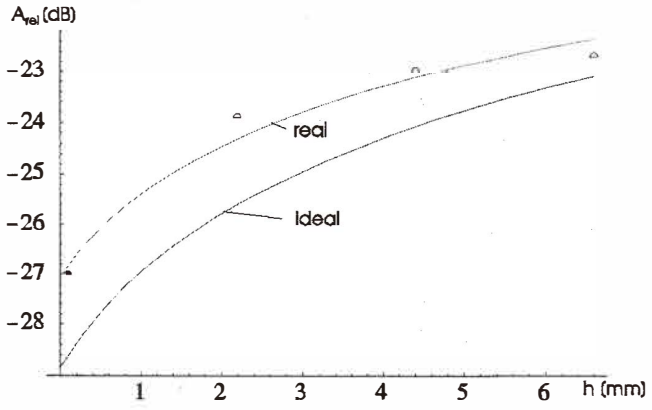

Fig. 18. Amplitude of the impedance-affected reflection relative to the reference (calculation and some measurement points).

Acknowledgments

The authors are grateful to Professor G. Fasching and Professor F. Seifert for making these investigations possible. The research was carried out under the Faculty of Electrical Engineering and Information Technology Top Priority Sensorics and Packaging at the Vienna University of Technology. Financial support was provided by Securiton Electronics, Vienna. The support of the SAW division ZT KM 1 of Siemens Corporate Research, Munich, is gratefully acknowledged. Authors would also like to thank Professor J. Korvink for inviting them to submit this paper to *Sensors and Materials*.

References

1 D. A. Thomson, L. T. Romankiw and A. F. Mayadas: IEEE Trans. Magn. **11** (1975) 1039.
2 P. Aigner, G. Stangl and H. Hauser: J. Phys. IV **8** (1998) 461.

3 M. N. Baibich, J. M. Brott, A. Fert, F. Nguyen, van Dau, F. Petroff, P. Etience, G. Cruzet, A. Friederich and J. Chazelas: Phys. Rev. Lett. **61** (1988) 2472.
4 H. Hauser, J. Nicolics, H. Bruggraber and H. Newald: Proc. 20th Spring Seminar on Electronic Technology (ISSE '97); (Szklarska Poreba, 1997) p. 152.
5 K. Mohri: Studies in Applied Electromagnetic and Mechanics **10** (1996) 634.
6 L. V. Panina and K. Mohri: J. Magn. Magn. Mater. **157** (1996) 137.
7 L. V. Panina and K. Mohri: Appl. Phys. Lett. **65** (1994) 1189.
8 H. Hauser and P. Fulmek: IEEE Trans. Magn. **28** (1992) 1815.
9 R. Steindl, C. Hausleitner, A. Pohl, H. Hauser and J. Nicolics: Sensors & Actuators A **85** (2000) 169.
10 H. Hauser and H. Newald: ÖVE Schriftenreihe **5** (1993) 126.
11 H. Hauser, R. Steindl, C. Hausleitner, A. Pohl and J. Nicolics: IEEE Trans. Instrum. Meas. **49** (2000) 648.
12 D. P. Morgan: Surface Wave Device for Signal Processing (Elsevier, Amsterdam, 1985).
13 F. Seifert, W. E. Bulst and C. C. W. Ruppel: Sensors & Actuators **44** (1994) 231.
14 R. Steindl, A. Pohl, L. Reindl and F. Seifert: Proc. IEEE Ultrasonic Symposium (1998).
15 A. Pohl: Proc. IEEE Frequency Control Symposium (1999) in print.
16 A. Pohl, R. Steindl, F. Seifert and W. E. Bulst: Reifen mit einem Sensor sowie Verfahren zur Bestimmung einer Verschleissgroesse eines solchen Reifens. European Patent Application 02/2000.